Simultaneous Synthesis of Au and Cu Nanoparticles in Pseudo-Core−Shell Type Arrangement Facilitated by DMPG and 12-6-12 Capping Agents

Mandeep Singh Bakshi,*[,†,‡,§,#] Fred Possmayer,[†,‡] and Nils O. Petersen[‡,§,||]

Department of Obstetrics and Gynaecology, Department of Biochemistry, and Department of Chemistry, University of Western Ontario, 339 Windermere Rd, London, ON, Canada N6A 5A5, National Institute for Nanotechnology, Edmonton, Alberta, Canada, and Department of Chemistry, Guru Nanak Dev University, Amritsar 143005, Punjab, India

Received November 20, 2006. Revised Manuscript Received January 8, 2007

A seed-growth method has been applied to synthesize the gold (Au) nanoparticles (NP) in the presence of 1,2-dimyristoyl-*sn*-glycero-3-[phospho-*rac*-(1-glycerol)] (sodium salt) (DMPG) and hexamethylene-1,6-bis(dodecyldimethylammonium bromide)(12-6-12) as capping agents at ambient conditions. The systematic addition of $CuSO_4$ leads to anisotropic growth of Au NP at low $CuSO_4$ concentration in the presence of DMPG while this was not observed in the case of 12-6-12 where mostly spherical Au NP were obtained. At high $CuSO_4$ concentration, small Cu NP appeared which arranged themselves around large Au NP in a typical pseudo-core−shell type arrangement. This was achieved by the fusion of lipid bilayers of lipid-capped Au and Cu NP. The cause of anisotropic growth of Au NP in the presence of DMPG has been discussed on the basis of its poor capping ability in comparison to 12-6-12.

Introduction

Recent advances in the synthesis of nanosized metallic morphologies have provided a variety of strategies to explore their vast applications in nanotechnology.[1] The shape and size-controlled synthesis of single-component nanoparticles (NP) such as Au, Ag, Ir, Pd, and Pt has generated immense interest in the field of nanoscience.[2] The synthesis of bimetallic NP is another very important branch of nanoscience where different metallic substances can be put together to produce integrated morphologies in a controlled fashion. The overall shape and structure of a bimetallic NP can then be manipulated by adjusting the material parameters of individual components. As physical properties significantly depend on the size of NP at nanoscale, any change in the size upon mixing two components leads to a drastic change in the physical properties. It provides numerous possibilities for achieving new combinations.[3]

The seed-mediated approach in producing shape-controlled Au NP in aqueous surfactant solutions has become increasingly popular recently.[4] Unlike the use of strong reducing agents, a controlled growth requires weak reducing conditions. Some studies have successfully lead to a controlled size distribution (typically 10−15%) in the range of 5−40 nm, and the size can be manipulated by varying the ratio of seed to metal salt.[5] Step-by-step size control is more effective than a single-step seeding method to avoid secondary nucleation. In seed-growth methods, small metal particles

* To whom correspondence should be addressed. E-mail: ms_bakshi@yahoo.com.
† Department of Obstetrics and Gynaecology, University of Western Ontario.
‡ Department of Biochemistry, University of Western Ontario.
§ Department of Chemistry, University of Western Ontario.
|| National Institute for Nanotechnology.
Guru Nanak Dev University.

(1) (a) *Handbook of Nanostructured Materials and Nanotechnology*; Nalwa, H. S., Ed.; Academic Press: New York, 2000. (b) *Nanostructured Materials: Clusters, Composites and Thin Films*; Shalaev, V. M., Moskovits, M., Eds.; American Chemical Society: Washington, DC, 1997.

(2) (a) Schneider, S.; Halbig, P.; Grau, H.; Nickel, U. *Photochem. Photobiol.* **1994**, *60*, 605. (b) Watzky, M. A.; Finke, R. G. *Chem. Mater.* **1997**, *9*, 3083. (c) Brown, K. R.; Natan, M. J. *Langmuir* **1998**, *14*, 726. (d) Brown, K. R.; Walter, D. G.; Natan, M. J. *Chem. Mater* **2000**, *12*, 306. (e) Henglein, A.; Giersig, M. *J. Phys. Chem. B* **1999**, *103*, 9533. (f) Henglein, A. *Langmuir* **1999**, *15*, 6738. (g) Teranishi, T.; Miyake, M. *Chem. Mater.* **1998**, *10*, 594. (h) Teranishi, T.; Hosoe, M.; Tanaka, T.; Miyake, M. *J. Phys. Chem. B* **1999**, *103*, 3818.

(3) (a) Kariuki, N. N.; Luo, J.; Maye, M. M.; Hassan, S. A.; Menard, T.; Naslund, H. R.; Lin, Y.; Wang, C.; Engelhard, M. H.; Zhong, C. J. *Langmuir* **2004**, *20*, 11240−11246. (b) Pasricha, R.; Swami, A.; Sastry, M. *J. Phys. Chem.* **2005**, *109*, 19620. (c) Shankar, S. S.; Rai, A.; Ahmad, A.; Sastry, M. *J. Colloid Interface Sci.* **2004**, *275*, 496. (d) Shibata, T.; Bunker, B. A.; Zhang, Z.; Meisel, D.; Vardeman, C. F., II; Gezelter, J. D. *J. Am. Chem. Soc.* **2002**, *124*, 11989. (e) Srnova-Sloufova, I.; Vlckova, B.; Bastl, Z.; Hasslett, T. L. *Langmuir* **2004**, *20*, 3407. (f) Yang, J.; Lee, J. Y.; Chen, L. X.; Too, H. P. *J. Nanosci. Nanotechnol.* **2005**, *5*, 1095.

(4) (a) Jana, N. R.; Gearheart, L.; Murphy, C. J. *J. Phys. Chem. B* **2001**, *105*, 4065. (b) Jana, N. R.; Gearheart, L.; Murphy, C. J. *Langmuir* **2001**, *17*, 6782. (c) Gole, A.; Murphy, C. J. *Chem. Mater.* **2004**, *16*, 3633. (d) Nikoobakht, B.; El-Sayed, M. A. *Langmuir* **2001**, *17*, 6368. (e) Swami, A.; Kumar, A.; Sastry, M. *Langmuir* **2003**, *19*, 1168. (f) Zana, N. R. *Small* **2005**, *1*, 875. (g) Bakshi, M. S.; Kaura, A.; Kaur, G.; Torigoe, K.; Esumi, K. *J. Nanosci. Nanotechnol.* **2006**, *6*, 644. (h) Bakshi, M. S.; Kaura, A.; Bhandari, P.; Kaur, G.; Torigoe, K.; Esumi, K. *J. Nanosci. Nanotechnol.* **2006**, *6*, 1405. (i) Kou, X.; Zhang, S.; Tsung, C. K.; Yeung, M. H.; Shi, Q.; Stucky, G. D.; Sun, L.; Wang, J.; Yan, C. *J. Phys. Chem.* **2006**, *110*, 16377. (j) Liu, M.; Guyot-Sionnest, P. *J. Phys. Chem.* **2005**, *109*, 22192. (k) Petkov, N.; Stock, N.; Bein, T. *J. Phys. Chem.* **2005**, *109*, 10737. (l) Shi, W.; Sahoo, Y.; Swihart, M. T.; Prasad, P. N. *Langmuir* **2005**, *21*, 1610. (m) Wei, Z.; Zamborini, F. P. *Langmuir* **2004**, *20*, 11301. (n) Brown, K. R.; Natan, M. J. *Langmuir* **1998**, *14*, 726.

(5) (a) Jana, N. R.; Gearheart, L.; Murphy, C. J. *Chem. Mater* **2001**, *13*, 2313. (b) Sau, T. K.; Pal, A.; Jana, N. R.; Wang, Z. L.; Pal, T. *J. Nanopart. Res.* **2001**, *3*, 257. (c) Meltzer, S.; Resch, R.; Koel, B. E.; Thompson, M. E.; Madhukar, A.; Requicha, A. A. G.; Will, P. *Langmuir* **2001**, *17*, 1713.

10.1021/cm062771t CCC: $37.00
Published on Web 02/17/2007

Scheme 1. Molecular Structures of DMPG and 12-6-12

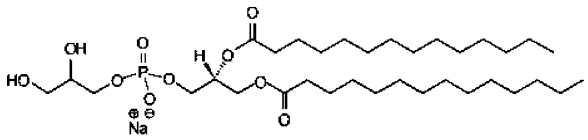

DMPG

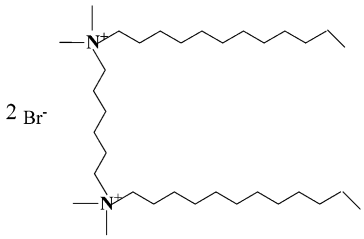

12-6-12

are prepared first and are later used as seeds (nucleation centers) for the preparation of larger size particles. Template-directed synthesis represents a convenient route to synthesize 1D nanostructures. In this approach, template mainly acts as a blueprint for a nanomaterial which is shaped into a nanostructure with its morphology complementary to that of the template. In a chemical process, the template is usually consumed as reaction proceeds and it is possible to directly obtain nanostructures as pure products.

Surfactants have been commonly utilized as templates in the synthesis of NP. Charged surfactants have also been used as stabilizers and templates for the growth of a variety of semiconductor and metallic nanodots.[6] Mostly, ionic monomeric surfactants such as cetyltrimethylammonium bromide (CTAB) and sodium dodecylsulfate (SDS) have been frequently used as capping as well as micellar templates at high surfactant concentrations. In comparison to ionic surfactants, gemini surfactants and phospholipids can be used as efficient capping agents in relatively much lower concentrations.[7] In this report, a simple, convenient, and room-temperature synthesis of Au and Cu NP has been reported by using DMPG (a phospholipid) and 12-6-12 (a cationic gemini surfactant) as capping agents (Scheme 1). DMPG belongs to a category of lipids with phospho-glycerol head group and is available commercially as sodium salt. In aqueous phase, an ionic phospholipid is considered to act as a better capping agent in comparison to a nonionic with phosphocholine head group. DMPG has been found to facilitate a well-defined pseudo-core−shell type arrangement among Au and Cu NP.

Experimental Section

Materials. Tetrachloroauric acid ($HAuCl_4$), sodium borohydride ($NaBH_4$), and trisodium citrate (Na3Cit) were obtained from Aldrich. 1,2-Dimyristoyl-*sn*-glycero-3-[phospho-*rac*-(1-glycerol)] (sodium salt) (DMPG) (14:0) with twin hydrophobic tails of 14 carbons each and no unsaturation was procured from Avati Polar Lipids. Hexamethylene-1,6-bis(dodecyldimethylammonium bromide)-(12-6-12) was synthesized as reported in the literature[8] and was used after repeated crystallization from ethanol. The molecular structures of both DMPG and 12-6-12 have been shown in Scheme 1. Ultrapure water (18 MΩcm) was used for all aqueous preparations.

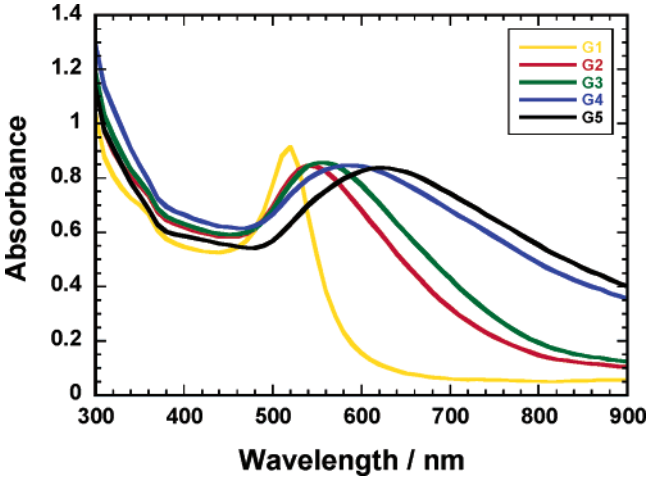

Figure 1. UV−vis spectra of aqueous gold nanoparticle solutions in the presence of DMPG ([DMPG] = 0.035 mM). [$CuSO_4$] = 0 mM (G1); [$CuSO_4$] = 0.1 mM (G2); [$CuSO_4$] = 0.2 mM (G3); [$CuSO_4$] = 0.4 mM (G4); [$CuSO_4$] = 0.4 mM and seed from sample G4 (G5) (see details in the text).

Preparation of DMPG/12-6-12 Capped Au and Cu Nanoparticles by Seed-Growth (S-G) Method. In an S-G method, the first step includes the preparation of a seed solution. First of all, 20 mL of $HAuCl_4$ aqueous solution ([$HAuCl_4$] = 0.5 mM) was taken in a screw-capped glass bottle and Na3Cit was added in it so as to make final concentration of [Na3Cit] = 0.5 mM. Then, 0.6 mL of aqueous $NaBH_4$ ([$NaBH_4$] = 0.1 mol dm^{-3}) solution was added under constant stirring which provided a ruby red color to the final solution. This is our seed solution. The growth solution was prepared by taking 120 μL of DMPG (1 mg/mL) in chloroform in a screw-capped glass tube. The chloroform was evaporated under the flux of pure N_2 leaving a dried lipid film at the bottom of the tube. In this tube, 5 mL of pure water was added along with two to three small glass beads, and it was vortexed for a few minutes to completely disperse the lipid in aqueous phase with final [DMPG] = 0.035 mM. In the case of 12-6-12, an aqueous solution of 12-6-12 ([12-6-12] = 0.45 mM, critical micelle concentration = 1.2 mM[8a]) was prepared by adding white powder of 12-6-12 in 5 mL water. Once both DMPG and 12-6-12 aqueous solutions were prepared separately, then it was followed by the addition of $HAuCl_4$ so as to make [$HAuCl_4$] = 0.5 mM in each case. This gave a light-yellow color to the solution. Then, 0.5 mL of previously made seed solution was added and followed by 0.2 mL of freshly prepared ascorbic acid (AA) aqueous solution ([AA] = 0.1 M). The solutions turned deep ruby red and were mixed a couple of times by inverting the tube which was kept in the dark without disturbing for at least 2 days. The pH of the aqueous NP solutions was always close to neutral.

A similar procedure was adopted to simultaneously synthesize Cu NP along with Au NP. Here, the addition of $CuSO_4$ was carried out immediately after the addition of $HAuCl_4$ in the growth solution

(6) (a) Youn, H. C.; Baral, S.; Fendler, J. H. *J. Phys. Chem.* **1988**, *92*, 6320. (b) Tanori, J.; Pileni, M. P. *Langmuir* **1997**, *13*, 639. (c) Ying, Y.; Chang, S. S.; Lee, C. L.; Wang, C. R. C. *J. Phys. Chem. B* **1997**, *101*, 6661. (d) Chen, C. C.; Chao, C. Y.; Lang, Z. H. *Chem. Mater.* **2000**, *12*, 1516.

(7) (a) Hara, K. J.; Aihara, N.; Usui, K.; Torigoe, K. *J. Colloid Interface Sci.* **1998**, *208*, 578. (b) Zhang, L.; Sun, X.; Song, Y.; Jiang, X.; Dang, S.; Wang, E. *Langmuir* **2006**, *22*, 2838. (c) Bakshi, M. S.; Sharma, P.; Banipal, T. S.; Kaur, G.; Torigoe, K.; Petersen, N. O.; Possmayer, F. *J. Nanosci. Nanotechnol.* **2007**, *7*, 916. (d) Xu, J.; Han, X.; Liu, H.; Hu, Y. *J. Dispersion Sci. Technol.* **2005**, *26*, 473.

(8) (a) Zana, R.; Benrraou, M.; Rueff, R. *Langmuir* **1991**, *7*, 1072. (b) Wettig, S. D.; Verall, R. E. *J. Colloid Interface Sci.* **2001**, *244*, 377.

Table 1. Various Constituents of Samples G1−G10 and the Shape and Structure of Their Nanoparticles

sample no.	$[CuSO_4]/[HAuCl_4]$	capping agent	seed solution	NP-shape (arrangement)
G1	no $CuSO_4$	DMPG	Au	Au-spherical (pearl necklace)
G2	0.2	DMP	Au	Au-nanowire (pearl necklace)
G3	0.4	DMPG	Au	Au-spherical and polyhedral (pearl necklace) Cu-polyhedral
G4	0.8	DMPG	Au	Au-polyhedral (pearl necklace) Cu-polyhedral (pseudo-core−shell)
G5	0.8	DMPG	G4	Au-dendritic (pearl necklace) Cu-polyhedral (pseudo-core−shell)
G6	no $CuSO_4$	12-6-12	Au	Au-spherical
G7	0.2	12-6-12	Au	Au-spherical, few nanorods
G8	0.4	12-6-12	Au	Au-spherical, few nanorods
G9	0.8	12-6-12	Au	Au-spherical, few nanorods
G10	0.8	12-6-12	G9	Au-spherical, few nanorods

while the rest of the reaction sequence was the same as mentioned in the previous paragraph. Three concentrations of $CuSO_4$, namely, 0.1, 0.2, and 0.4 mM, were used separately for both DMPG as well as 12-6-12 capped NP. Table 1 explains the number of reactions carried out for DMPG and 12-6-12 and [Cu]/[Au] mole ratio used in each case. Finally, two more growth reactions (namely, G5 and G10) were carried out in a similar manner in which instead of using Au seed solution (which was used previously in each case), 0.5 mL of G4 and G9 for DMPG and 12-6-12, respectively (Table 1), were used as seed solutions. The amount of $CuSO_4$ used in both reactions was 0.4 mM while all other ingredients were the same (Table 1). All reactions were carried out at room temperature under ambient conditions and the samples were purified from pure water at least three times after centrifugation at 10 000 rpm for 10 min. No liposomes were observed from transmission electron microscopy (TEM) studies after the purification process.

Methods. UV−vis spectra of as-prepared NP solutions were taken by UV spectrophotometer (Multiskan Spectrum, model no. 1500) in the wavelength range of 200−900 nm to determine the absorbance because of surface plasmon resonance (SPR). The formation of Au and Cu NP was monitored in the visible absorption range around 520 and 570 nm, respectively. The shape and size of Au and Cu NP were characterized by transmission electron microscopy (TEM). The samples were prepared by mounting a drop of NP solution on a carbon-coated Cu grid and allowing it to dry in air. They were observed with the help of a Philips CM10 transmission electron microscope operating at 100 kV. The chemical composition of some samples containing Au and Cu NP was confirmed with the help of X-ray photon spectroscopic (XPS) measurements. A portion of an aqueous NP solution was placed onto a clean silicon wafer, and then it was put into the introduction chamber of the XPS instrument. The liquid was then pumped away. The sample was analyzed by using a Kratos Axis Ultra X-ray photoelectron spectrometer. XPS can detect all elements except hydrogen and helium and can probe the surface of the sample to a depth of 7−10 nm. Survey scan analyses were carried out with an analysis area of 300 × 700 microns.

Gel Electrophoresis. The polarity of the lipid-capped NP was determined from the gel electrophoresis by using Tris-HCl buffer as a gel running medium with pH = 7. For this purpose, 1% of aqueous agrose solution was first microwave boiled and left in the gel plate to harden. Then, 20 μL of aqueous NP solution was loaded in each gel well and a direct voltage of 90 V was applied for 10 min to observe the movement of NP. No staining agent was used because NP solution in each case was colored (either ruby red or purple).

Results and Discussion

DMPG Capped Au and Cu NP. Synthesis of Au NP in aqueous DMPG solution in the absence of $CuSO_4$ was confirmed by measuring the UV−vis spectrum at ≈520 nm. Figure 1 shows a clear sharp absorbance at ≈520 nm because of the characteristic SPR of Au NP. As the amount of $CuSO_4$ increases from G2 to G4, the absorbance becomes broad and systematically shifts to higher wavelength. There is approximately 60-nm red shift from G2 to G4. On the other hand, when the NP solution of sample G4 is used as a seed solution for the preparation of G5, there is another 40-nm shift in the absorbance from that of sample G4 and more than 100-nm shift from that of G1. Figure 1 does not show any clear absorbance because of Cu NP which should be located somewhere between 550 and 600 nm depending on the size of Cu NP. Lisiecki and Pilani[9a] demonstrated a systematic dependence of SPR on the size of Cu NP. Small-size Cu NP (<10 nm) generally show a broad SPR located between 550 and 600 nm while larger NP give prominent and sharp SPR around 570 nm.[9b−d] This behavior is somewhat different from that of Au NP which show broad and red-shifted SPR when they undergo some sort of aggregation or anisotropic growth.[4a−c,7c] One would find in Figure 1 that the SPR of G3−G5 becomes systematically broad and shifts to higher wavelength. This can happen because of anisotropic growth and aggregation in the case of Au NP as well as because of the presence of Cu NP with size distribution less than 10 nm.

The corresponding TEM images of sample G1 are shown in Figure 2, where Figure 2a and its magnification (Figure 2b) show DMPG capped Au NP. They are arranged in a pearl-necklace type arrangement with size distribution 13.8 nm. When the same reaction is being carried out with a small amount of $CuSO_4$ ($[CuSO_4] = 0.1$ mM, sample G2), the Au NP merge with each in the form of nanowires (NW) with uniform thickness of 13 nm (Figure 3a). Figure 3b demonstrates a magnified view of a few branched NW where a few spherical NP merge with each other (shown by a circle) and take the form of an NW. One would find an almost equal size of spherical NP of G1 (Figure 2) and thickness of the NW of G2 (Figure 3). It suggests that the addition of $[CuSO_4] = 0.1$ mM in fact leads to a salt effect and no Cu NP are obtained. A transformation from spherical Au NP to NW formation can be explained on the basis of a shift in the crystal growth from {111} facets to {100}[10] by the addition of $CuSO_4$. It seems that the vesicles of DMPG in the aqueous

(9) (a) Lisiecki, I.; Pilani, M. P. *J. Am. Chem. Soc.* **1993**, *115*, 3887. (b) Creighton, J. A.; Eadon, D. G. *J. Chem. Soc., Faraday Trans.* **1991**, *87*, 3881. (c) Truong, V. V.; Scott, G. D. *J. Opt. Soc. Am.* **1977**, *67*, 502. (d) Anno, E.; Tanimoto, M.; Yamaguchi, T. *Phys. Rev. B* **1988**, *38*, 3521.

(10) (a) Ni, C.; Hassan, P. A.; Kaler, E. W. *Langmuir* **2005**, *21*, 3334. (b) Hong, B. H.; Bae, S. C.; Lee, C. W.; Jeong, S.; Kim, K. S. *Science* **2001**, *294*, 348.

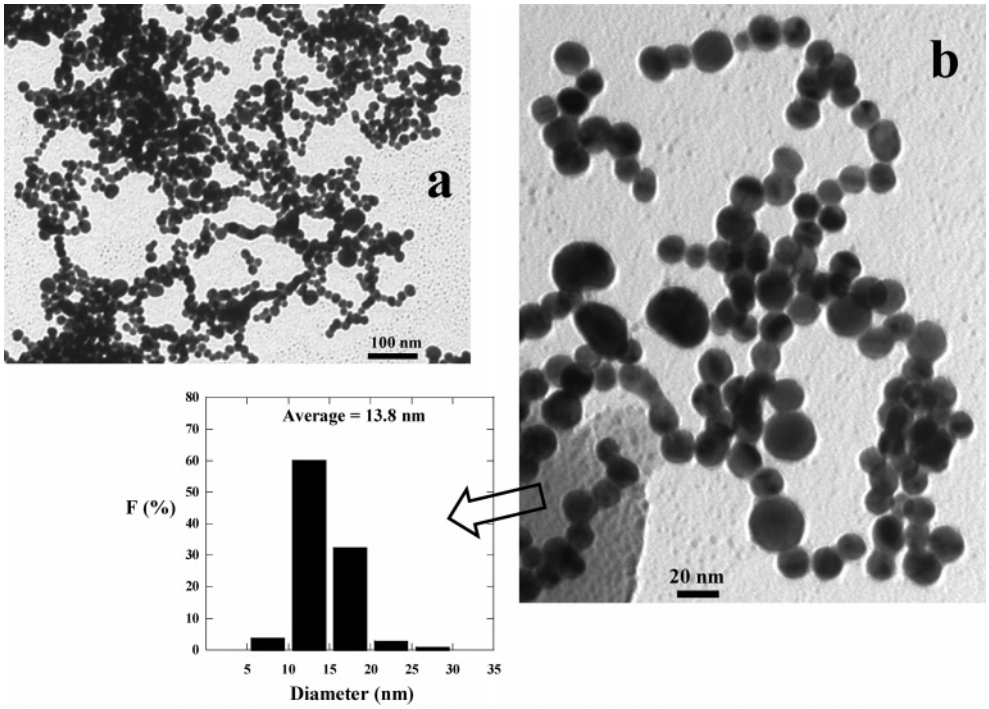

Figure 2. (a) TEM micrographs of gold nanoparticles in the presence of DMPG ([DMPG] = 0.035 mM) for sample G1 ([$CuSO_4$] = 0 mM); (b) shows the closeup view with pearl-necklace arrangement.

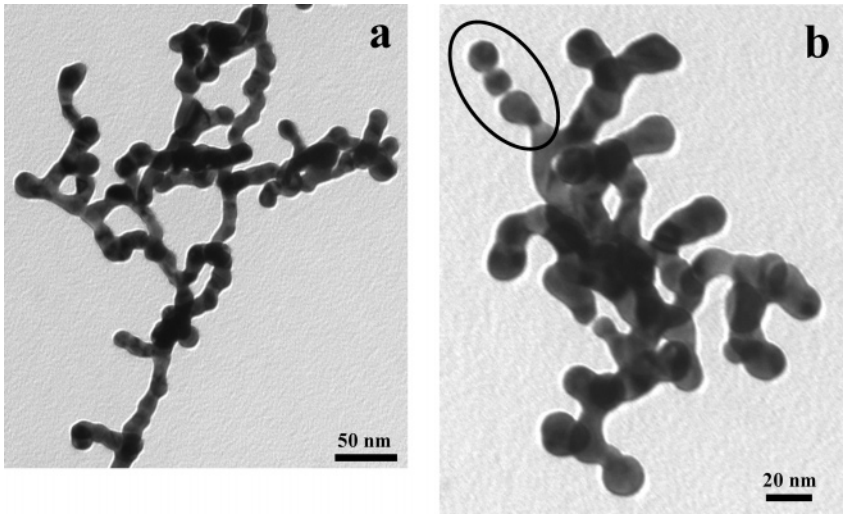

Figure 3. (a) TEM micrographs of clear gold nanowires in the presence of DMPG ([DMPG] = 0.035 mM) for sample G2 ([$CuSO_4$] = 0.1 mM); (b) a closeup view showing how spherical gold nanoparticles fused to form nanowires (in black circle).

phase are stabilized[11] by the addition of $CuSO_4$ (because of the salt effect) and with the result of which a relatively less amount of DMPG molecules is available to cap spherical Au NP leaving some uncapped facets for further growth. Thus, the uncapped facets of adjoining Au NP which already exist in the form of pearl-necklace model further undergo nucleation and ultimately merge with each other in the form of NW.

The increase in the amount of $CuSO_4$ ([$CuSO_4$] = 0.2 mM, sample G3) further reduces the capping ability of DMPG and opens up new facets for more nucleation. The size distribution histogram of Figure 4a demonstrates an average size of 22.7 nm Au NP. This is significantly larger in comparison to the size of spherical NP of sample G1 (Figure 2). However, apart from this, much larger Au NP have also been observed (Figure 4b) with size distribution 70.3 nm, which prefer to exist independently rather than in the form of pearl-necklace arrangement. A less amount of DMPG would leave some of the uncapped Au NP prone for {111} growth and consequently would lead to the formation of large Au NP.[11] Therefore, poorly capped large Au NP are not expected to arrange themselves in a pearl-necklace model because of the nonavailability of lipid bilayers around them. This sample also shows the presence of small Cu NP (light-shaded particles in white circles in Figure 4b).

As the concentration of $CuSO_4$ becomes double than that used for sample G3, a large density of small Cu NP are formed in sample G4. Sample G4 consists of [$CuSO_4$] = 0.4 mM, and its TEM images are shown in Figure 5. Figure

(11) (a) Luk, A. S.; Kaler, E. W.; Lee, S. P. *Biochemistry* **1997**, *36*, 5633. (b) Kawasaki, H.; Garamus, V. M.; Almgren, M.; Maeda, H. *J. Phys. Chem. B* **2006**, *110*, 10177.

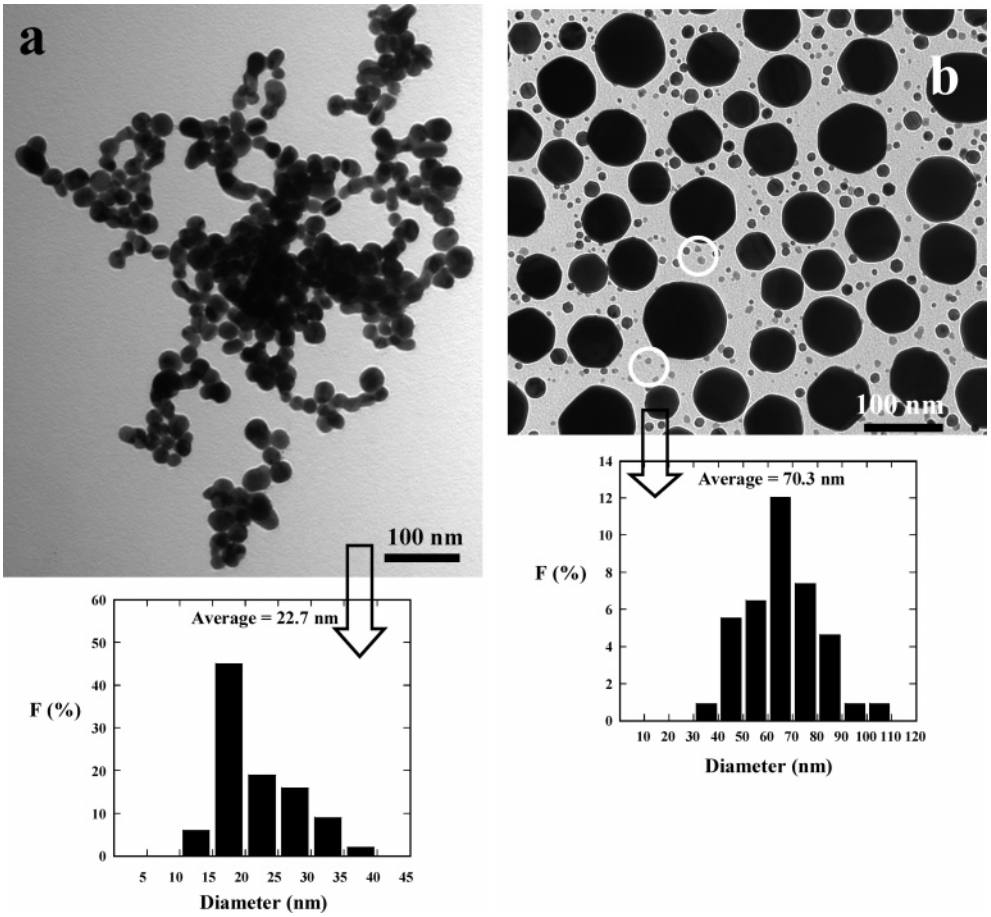

Figure 4. (a) TEM micrographs of gold nanoparticles in the presence of DMPG ([DMPG] = 0.035 mM) for sample G3 ([$CuSO_4$] = 0.2 mM) showing pearl-necklace arrangement; (b) shows very large gold nanoparticles with few light shaded copper nanoparticles (shown in white circles).

5a shows a pearl-necklace type arrangement of many Au NP with size distribution close to 22.1 nm. This size of Au NP is very close to that of sample G3 (Figure 4a), but shapes are clearly nonspherical and mostly polyhedral. Large Au NP with almost similar size distribution as observed in Figure 4b were also present in G4 (not shown). Thus, it suggests that the present amount of $CuSO_4$ mainly facilitates the formation of Cu NP (Figure 5c) with size distribution 4.7 nm. The presence of Cu NP can be easily confirmed by carrying out the same reaction in the absence of gold salt under identical reaction conditions. Supplementary Figure S1 shows the UV−vis spectrum of colloidal DMPG capped Cu NP with clear broad absorbance located around 520 nm because of the presence of small-size (<10 nm) NP. A corresponding TEM image (Figure S2) confirms the presence of Cu NP with average size distribution ≈4.2 nm. Figure 5b demonstrates a close inspection of Au NP where they are wrapped with less dark and much smaller Cu NP in a typical pseudo-core−shell type arrangement. The presence of Cu NP along with that of Au can be easily confirmed from the XPS measurements. Figure 6 shows the XPS spectra of NP of some samples and Table 2 lists the binding energies and atomic percent values. Each spectrum has been divided into two ranges of binding energies for the sake of clarity. Figure 6a shows the emission peaks due to Au 4f and Au 4d electrons. There is practically no shift in both kinds of peaks for G3 and G4 from that of G1 indicating no Au−Cu bimetallic NP formation.[12a] Figure 6b, on the other hand, shows the emission peaks due to Cu 2p3/2 and Cu 2p1/2 electrons,[12b,c] and another at 570 eV is due to Cu auger. The former peaks are located around 932 eV (Table 2) and are at least more than 1 eV lower than that typical of CuO. This thus removes any possibility of oxidation of Cu NP in the form of CuO. Therefore, Cu 2p peaks listed in Table 2 indicate that the valence state of Cu in our samples lies between 0 and +1. The intensities of these peaks for sample G4 are clearly higher than that of G3 suggesting the presence of a greater amount of Cu NP in the former sample (Table 2). The binding energies in all the cases do not show any shift in the emission peaks indicating the absence of Au−Cu bimetallic NP. Therefore, both figures (Figure 6a and 6b) suggest the presence of independent Au and Cu NP or, in other words, they exist in the form of pseudo-core−shell type arrangement as evident from TEM images.

Gel electrophoresis can be used to determine the charge on small monodisperse NP (Figure 7). Samples G1 and G2 do not show any displacement of their NP, but samples G3 and G4 demonstrate a significant shift of NP toward positively charged electrode under the effect of applied potential. The density of the displaced NP is much higher for sample G4 rather than for G3. Au NP (from sample G1 to G4) are always arranged in pearl-necklace model and are

(12) (a) Sangregorio, C.; Galeotti, M.; Bardi, U.; Baglioni, P. *Langmuir* **1996**, *12*, 5800. (b) Ang, T. P.; Wee, T. S. A.; Chin, W. S. *J. Phys. Chem. B* **2004**, *108*, 1101. (c) Laibinis, P. E.; Whitesides, G. M. *J. Am. Chem. Soc.* **1992**, *114*, 9022.

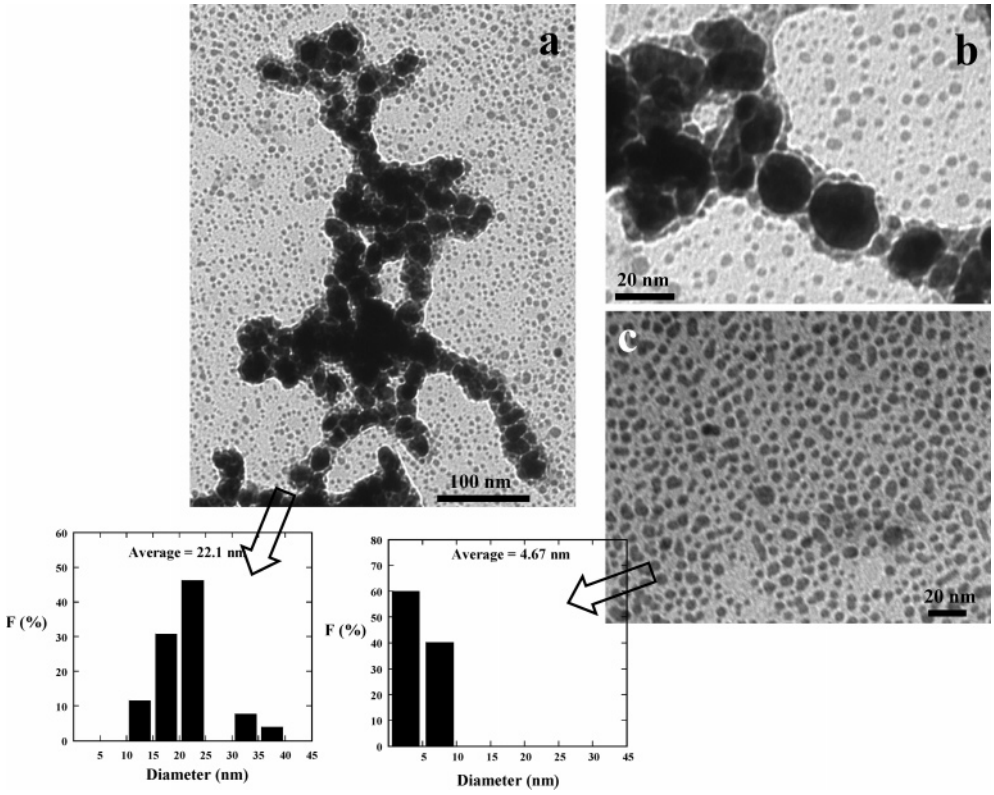

Figure 5. (a) TEM micrographs of gold and copper nanoparticles in the presence of DMPG ([DMPG] = 0.035 mM) for sample G4 ([$CuSO_4$] = 0.4 mM) showing pearl-necklace arrangement of gold nanoparticles which are completely covered by a continuous shell of copper nanoparticles; (b) shows a closeup view and has been termed as pseudo-core−shell type arrangement (see details in the text); (c) shows copper nanoparticles.

Table 2. Binding Energies/eV (*a*) and Results of XPS Analysis in Atomic Percent (*b*)

	Au 4f		Cu 2p		C 1s		N 1s	
sample	*a*	*b*	*a*	*b*	*a*	*b*	*a*	*b*
G1	84.5	2.0			284.7	52.5		
G3	84.5	1.7	932.6	0.4	284.7	28.8		
G4	84.5	5.7	932.2	2.0	284.7	38.5		
G10	87.6	0.4	932.1	0.4	285.0	44.3	401.9	2.4

not supposed to move through the gel phase while much smaller Cu NP capped with bilayer of anionic lipid (DMPG) can easily move through the gel phase. Since sample G4 contains a much greater number of Cu NP, a greater density of Cu NP moves toward the positively charged electrode.

Interestingly, when sample G4 is used as a seed for further growth for sample G5 while keeping the $CuSO_4$ concentration the same as that used in sample G4 (i.e., [$CuSO_4$] = 0.4 mM), there is about a 3 times increase in the size of Au NP of G5 (i.e., 56.9 nm) from that of G4 while the size of the Cu NP remains almost the same (Figure 8). The polyhedral structure of Au NP of sample G4 converts into a dendritic type structure[13] in sample G5. Recently, some studies have reported that the origin of such kind of morphologies is due to the shape-directing agents (a surfactant or a salt like sodium citrate) which preferentially adsorb at some specific crystal planes and lead to the intrinsic crystal growths.[13,14] An uneven branch growth is considered to be kinetic-controlled phenomenon[13a,14] and hence the growth directions are nonspecific. In the present work, therefore, the shape-directing effect of citrate ions is also considered to be a contributing factor especially in the presence of $CuSO_4$ which reduces the capping ability of DMPG. This leaves some of the crystal planes available for citrate shape-directing agent to facilitate further nucleation under the kinetic effects. The dendritic Au NP in this sample are also covered with a thin shell of small Cu NP (Figure 8b). The driving force for this kind of pseudo-core−shell type arrangement comes from the fusion of lipid-capped DMPG bilayers. DMPG is a saturated phospholipid with two fatty acid hydrocarbon tails consisting of 14 carbons in each case (Scheme 1). It provides both charge as well as steric stabilizations[15] for Au and Cu colloidal NP. When DMPG capped Au and Cu NP come in contact with each other through lipid bilayers, the amphipathic interactions between the bilayers of neighboring NP act as binder.[16] This brings much smaller Cu NP in the form of shell around large Au NP as shown schematically in Figure 9. The whole growth sequence from G1 to G5 indicates no evidence of any Au−

(13) (a) Sau, T. K.; Murphy, C. J. *J. Am. Chem. Soc.* **2004**, *126*, 8648. (b) Wu, H. Y.; Liu, M.; Huang, M. H. *J. Phys. Chem. B* **2006**, *110*, 19291. (c) Bakr, O. M.; Wunsch, B. H.; Stellacci, F. *Chem. Mater.* **2006**, *18*, 3297. Kuo, C. H.; Huang, M. H. *Langmuir* **2005**, *21*, 2012.

(14) (a) Teng, X.; Yang, H. *Nano Lett.* **2005**, *5*, 885. (b) Chen, J.; Herricks, T.; Xia, Y. *Angrew. Chem., Int. Ed.* **2005**, *44*, 2589.

(15) (a) Roucoux, A.; Schulz, J.; Patin, H. *Chem. Rev.* **2002**, *102*, 3757. (b) Napper, H. D. In *Polymeric Stabilization of Colloidal Dispersions;* Academic Press: London, 1983. (c) Lin, Y.; Finke, R. G. *J. Am. Chem. Soc.* **1994**, *116*, 8335.

(16) (a) Jenkins, A. T. A.; Bushby, R. J.; Evans, S. D.; Knoll, W.; Offenhausser, A.; Ogier, S. D. *Langmuir* **2002**, *18*, 3176. (b) Ross, E. E.; Spratt, T.; Liu, S.; Rozanski, L. J.; O'Brien, D. F.; Saavedra, S. S. *Langmuir* **2003**, *19*, 1766. (c) Berquand, A.; Mazeran, P. E.; Pantigny, J.; Proux-Delrouyre, V.; Laval, J. M.; Bourdillon, C. C. *Langmuir* **2003**, *19*, 1700.

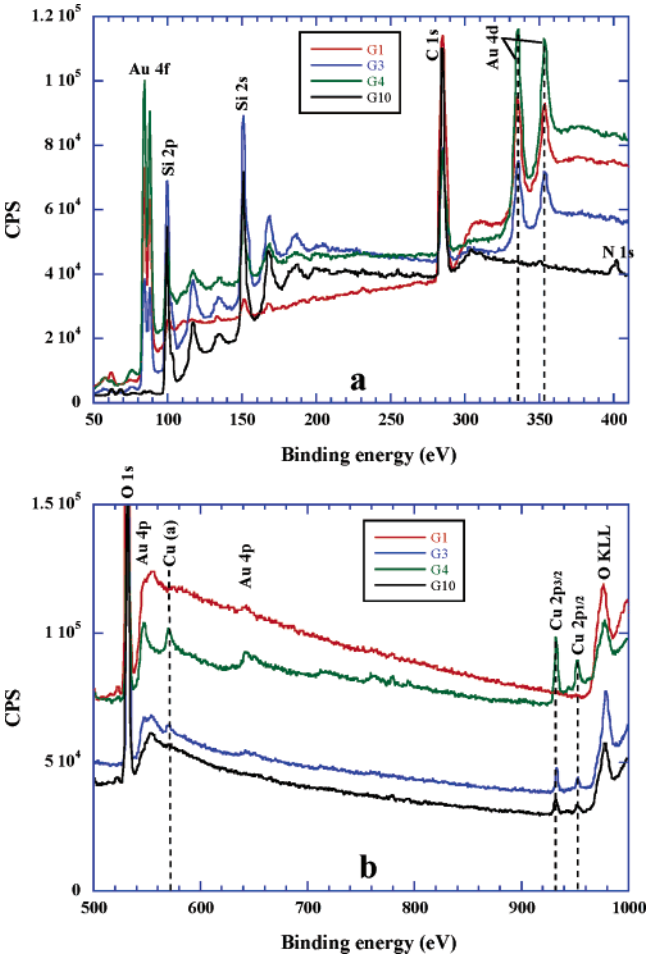

Figure 6. XPS spectra of samples G1, G3, G4, and G10.

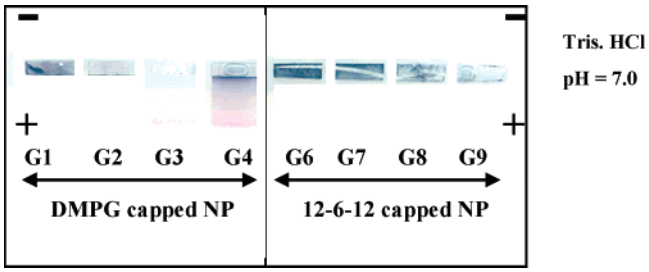

Figure 7. Gel electrophoresis of samples G1−G5 and G7−G9.

Cu bimetallic NP formation. Thus, the results demonstrate that $CuSO_4$ mainly acts as a salt additive, and an increase in its amount only causes a change in the capping ability of DMPG as a consequence of which the shape and size of Au NP change apart from getting small Cu NP at high $CuSO_4$ concentration.

12-6-12 Capped Au and Cu NP. Figure 10 shows the absorbance of Au NP capped with 12-6-12. Unlike DMPG, here the increase in concentration of $CuSO_4$ does not significantly affect the SPR of Au NP. There is about a 30-nm red shift in the SPR, and it remains more or less constant (∼550 nm) for G7−G9 at different $CuSO_4$ concentrations. However, when G9 is used as seed for samples G10, there is a large increase in SPR with a red shift of 30 nm. The TEM images of samples G6 and G9 have been shown in Figure 11a and 11b, respectively, with corresponding size distribution 17.1 nm and 14.2 nm. It seems that there is not much difference between the size and shape of NP of both samples, but the NP of G9 are mainly arranged in a pearl-necklace model and that could be the reason of a red shift in SPR of G9. Apart from this, there is no sign of Cu NP presence, and even the gel electrophoresis does not show any displacement of NP of samples G7−G9 (Figure 7). On the contrary, TEM image of sample G10 (Figure 12) shows large spherical Au NP with some scattered nanorods (NR) of average aspect ratio 1.9 (shown by white block arrows). The size of spherical NP is increased dramatically and the size distribution histogram shows an average size around 37.6 nm. This sample also shows several clear Cu NP scattered around large Au NP though their density seems to be much higher at the surface of Au NP with no clear pseudo-core−shell type arrangement. Thus, the red shift in the SPR of G10 (Figure 10) was collectively due to the presence of large Au NP and small Cu NP. The Cu NP of this sample too did not show any displacement under gel electrophoresis (not shown). The XPS spectrum of this sample (Figure 6) shows the presence of independent Cu and Au NP as demonstrated for samples G3 and G4.

All the above results indicate that there is some fundamental difference between the capping ability of DMPG and 12-6-12. The first difference is that the DMPG is anionic lipid while 12-6-12 is a dimeric cationic surfactant[8,17] (Scheme 1). The oppositely charged DMPG and 12-6-12 ions should have an entirely different capping mechanism in the growth process. In the case of DMPG, the Na^+ ions are expected to interact first with the negatively charged citrate-stabilized Au NP surface and that should be followed by the electrostatic interactions with negatively charged DMPG anions. On the contrary, the dimeric cationic head group of 12-6-12 would directly interact with the Au NP surface rather than Br^- ions. Thus, strong electrostatic interactions between dimeric cationic head group of 12-6-12 and negatively charged Au NP will instantaneously provide both charge as well as steric stabilization[15] to NP whereas such interactions are not expected to be so strong in the case of DMPG. Hence, the capping ability in the case of DMPG is not considered to be as strong as in the case of 12-6-12 since the former is interacting electrostatically to the NP surface through already created electrical double layer. Apart from this, DMPG vesicular phase itself is quite stable and would leave a relatively less amount of DMPG monomers available for bilayer capping ability in comparison to a more fluid micellar phase of 12-6-12. All these factors coupled with a relatively less amount of DMPG (0.035 mM) used than that of 12-6-12 (0.45 mM) provides less amount of DMPG for capping in comparison to 12-6-12. The choice of low DMPG concentration was to avoid the formation of multilayer vesicles which were found difficult to remove during the NP purification to get clear TEM images. Even a higher concentration of DMPG has shown a little effect on the shape and structure of NP (not shown) which suggested that the

(17) (a) Bakshi, M. S.; Singh, K.; Kaur, G.; Yoshimura, T.; Esumi, K. *Colloids Surf.* **2006**, *278*, 129. (b) Bakshi, M. S.; Singh, K.; Singh, J. *J Colloid Interface Sci.* **2006**, *297*, 284. (c) Bakshi, M. S.; Sachar, S. *J. Colloid Interface Sci.* **2006**, *296*, 309. (d) Bakshi, M. S.; Singh, J.; Kaur, G. *Chem. Phys. Lipids* **2005**, *138*, 81. (e) Bakshi, M. S.; Singh, J.; Kaur, G. *J. Photochem. Photobiol.* **2005**, *173*, 202.

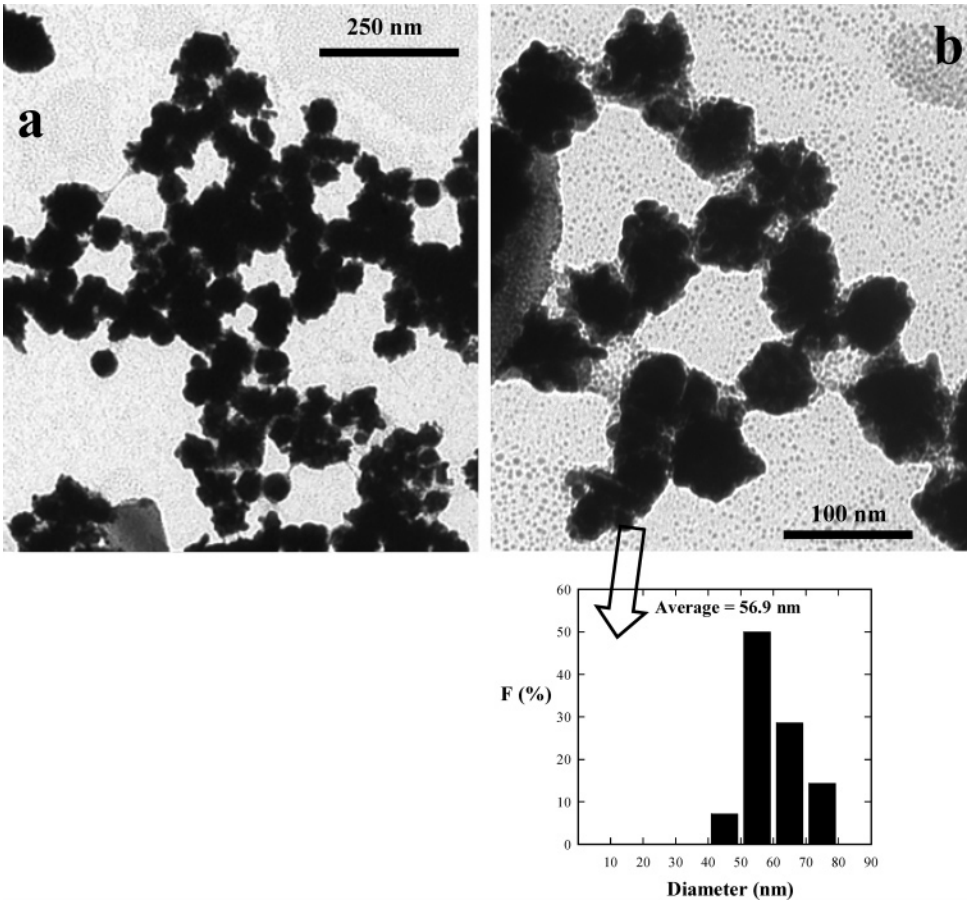

Figure 8. (a) TEM micrographs of gold and copper nanoparticles in the presence of DMPG ([DMPG] = 0.035 mM) for sample G5 ([$CuSO_4$] = 0.4 mM) showing pearl-necklace arrangement of large dendritic gold nanoparticles which are completely covered by a continuous shell of copper nanoparticles; (b) shows a closeup view (see details in the text).

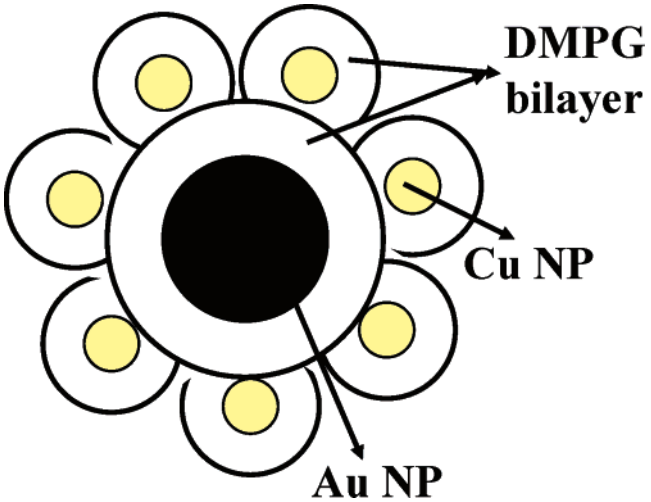

Figure 9. A schematic representation of pseudo-core−shell type arrangement of gold and copper nanoparticles facilitated by the DMPG bilayers.

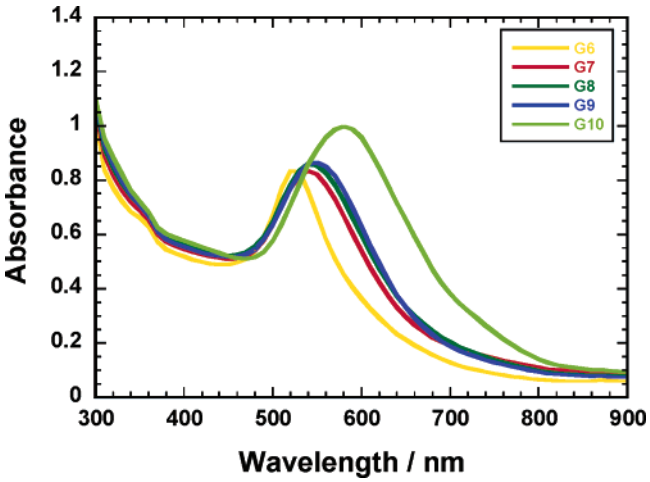

Figure 10. UV−vis spectra of aqueous gold nanoparticle solutions in the presence of 12-6-12 ([12-6-12] = 14 mM). [$CuSO_4$] = 0 mM (G6); [$CuSO_4$] = 0.1 mM (G7); [$CuSO_4$] = 0.2 mM (G8); [$CuSO_4$] = 0.4 mM (G9); [$CuSO_4$] = 0.4 mM and seed from sample G9 (G10) (see details in the text).

excess amount of DMPG was accommodating in vesicle formation.

Addition of $CuSO_4$ initially acts as a salt additive and stabilizes the vesicular and micellar structures[11,18] of DMPG and 12-6-12, respectively. Since equal amounts of $CuSO_4$ have been used in the synthesis of Au NP in the presence of both DMPG and 12-6-12, a relatively less amount of $CuSO_4$ will stabilize the vesicles of DMPG in comparison to that which would stabilize the micelles of 12-6-12. This will keep more Cu^{+2} ions in aqueous DMPG rather than in aqueous 12-6-12. That is why the Cu NP were first observed at [$CuSO_4$] = 0.2 mM in sample G3 (Figure 4b), while no Cu NP were observed even at [$CuSO_4$] = 0.4 mM in sample G8 (Figure 11b). The atomic percent of Cu 2p obtained from XPS even for sample

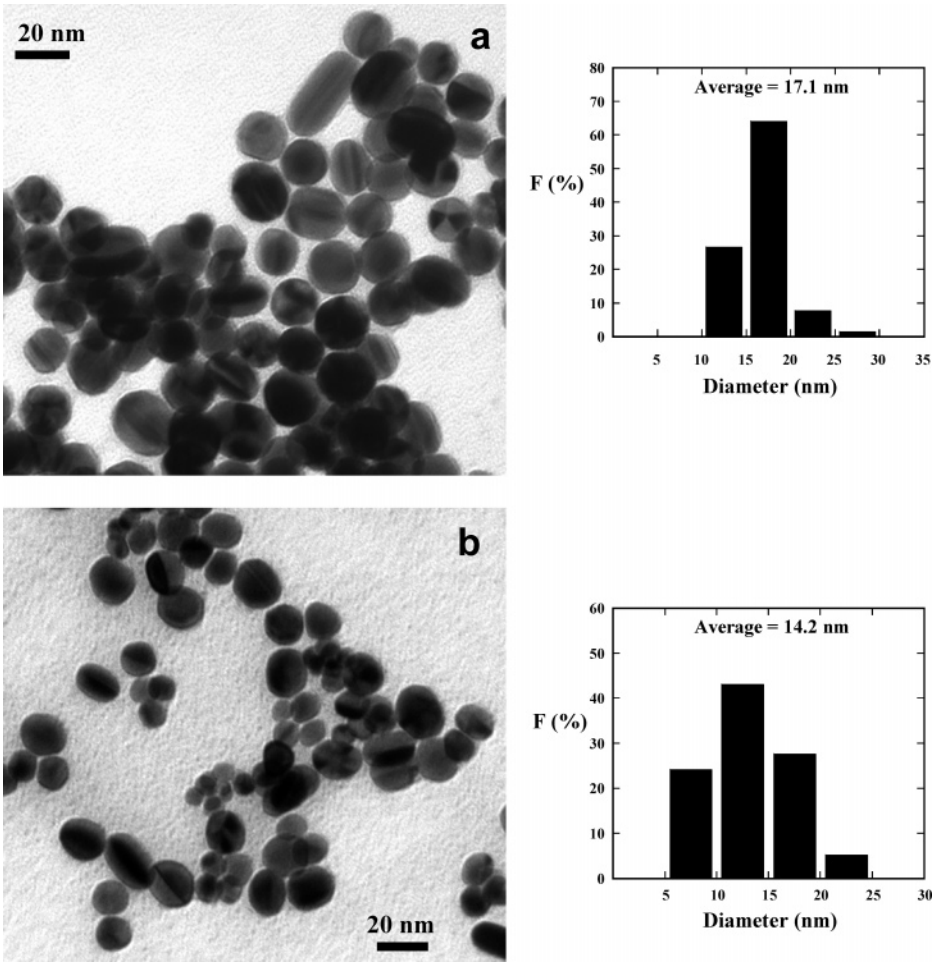

Figure 11. (a) TEM micrographs of gold nanoparticles in the presence of 12-6-12 ([12-6-12] = 14 mM) for sample G6 ([$CuSO_4$] = 0 mM) and for sample G9 ([$CuSO_4$] = 0.4 mM) (see details in the text).

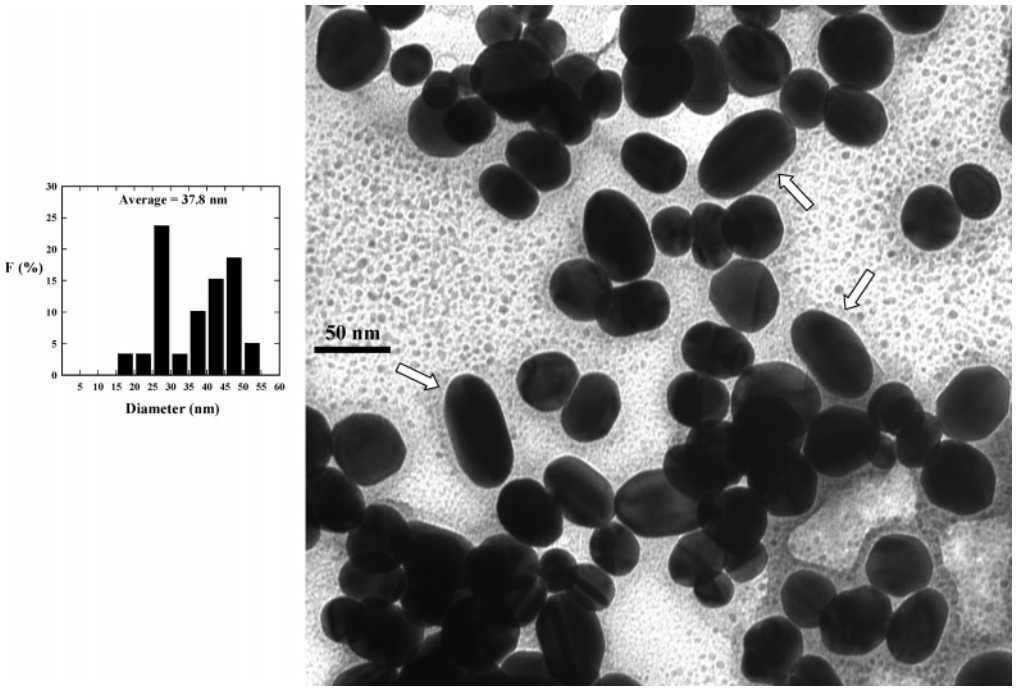

Figure 12. (a) TEM micrographs of gold and copper nanoparticles in the presence of 12-6-12 ([12-6-12] = 14 mM) for sample G10 ([$CuSO_4$] = 0.4 mM). The white arrows show gold nanorods (see details in the text).

G10 was equivalent to G3 (Table 2). Hence, a major difference between the capping ability of DMPG and 12-6-12 in the presence of $CuSO_4$, therefore, governs overall shape and size of Au NP while fusion of DMPG bilayers of Au and Cu NP is mainly responsible for pseudo-core−shell arrangement.

Conclusions

Au NP synthesized in the presence of DMPG always arrange themselves in a typical pearl-necklace type arrangement while this is not so significant in the presence of 12-6-12. The mutual interactions between the bilayers of adjoining NP are thought to be responsible for the peal-necklace type arrangement in the former case.

Addition of $CuSO_4$ has dramatic influence on the morphology of Au NP in the presence of DMPG whereas this effect is almost insignificant in the case of 12-6-12. It has been concluded that $CuSO_4$ acts as a salt additive and its presence reduces the effective amount of DMPG available for the capping process because of its vesicle stabilization effect. This leaves some of the crystal planes uncapped and open for anisotropic growth which leads to the formation of fine nanowires at low $CuSO_4$ concentration. High $CuSO_4$ concentration leads to an increase in the size of Au NP and also produces DMPG capped Cu NP. Both Au and Cu DMPG capped NP when coming in contact with each other arrange themselves in a typical pseudo-core−shell type arrangement. The core is constituted by a large Au NP while the shell consists of several small Cu NP. A similar arrangement is not observed in the case of 12-6-12, where increasing concentration of $CuSO_4$ shows little influence on the shape and structure of Au NP.

Acknowledgment. M.S. Bakshi thanks financial assistance from CCP (Centre for Chemical Physics) and CIHR (Canadian Institutes of Medical Research, MOP 64406). The authors also thank R. Smith (Dept of Biology, UWO) for his kind help in getting the TEM micrographs.

Supporting Information Available: UV−vis spectra and TEM image of aqueous copper NP solutoin in the presence of DMPG. This material is available free of charge via the Internet at http://pubs.acs.org.

CM062771T

(18) (a) Okano, T.; Tamura, T.; Nakano, T. Y.; Ueda, S. I.; Lee, S.; Sugihara, G. *Langmuir* **2000**, *16*, 3777. (b) Hisatomi, M.; Abe, M.; Yoshino, N.; Lee, S.; Nagadome, S.; Sugihara, G. *Langmuir* **2000**, *16*, 1515. (c) Nagadome, S.; Okazaki, Y.; Lee, S.; Sasaki, Y.; Sugihara, G. *Langmuir* **2001**, *17*, 4405. (d) Manabe, M.; Funamoto, M.; Kohgami, F.; Kawamura, H.; Katsuura, H. *Colloid Polym. Sci.* **2003**, *281*, 239. (e) Manabe, M.; Tokunga, A.; Kawamura, H.; Katsuura, H.; Shiomi, M.; Hiramatsu, K. *Colloid Polym. Sci.* **2002**, *280*, 929. (f) Manabe, M.; Kaneko, M.; Miura, T.; Akiyama, C.; Kawamura, H.; Katsuura, H.; Shiomi, M. *Bull. Chem. Soc. Jpn.* **2002**, *75*, 1967. (g) Katsuura, H.; Kawamura, H.; Manabe, M.; Kawasaki, H.; Maeda, H. *Colloid Polym. Sci.* **2002**, *280*, 30.